

## ELECTRONIC SUPPLEMENTARY INFORMATION

### **Dual-Responsive Jumping Actuators by Light and Humidity**

Jingjing Li<sup>a,b\*</sup>, Meilin Wang<sup>c</sup>, Zhanpeng Cui<sup>c</sup>, Shiyong Liu<sup>c</sup>, Danyang Feng<sup>b</sup>, Guangkai Mei<sup>b</sup>,  
Rui Zhang<sup>d</sup>, Baigang An<sup>e</sup>, Dong Qian<sup>d</sup>, Xiang Zhou<sup>c\*</sup>, Zunfeng Liu<sup>b\*</sup>

<sup>a</sup>School of Textile Science and Engineering, Wuhan Textile University, Wuhan, Hubei, 430200,  
China

<sup>b</sup>State Key Laboratory of Medicinal Chemical Biology, Key Laboratory of Functional Polymer  
Materials, Frontiers Science Center for New Organic Matter, College of Chemistry, Nankai  
University, Tianjin 300071, China

<sup>c</sup>Department of Science, China Pharmaceutical University, Nanjing 211198, China

<sup>d</sup>Department of Mechanical Engineering, University of Texas at Dallas, Richardson, TX 75080,  
USA

<sup>e</sup>School of Chemical Engineering, University of Science and Technology Liaoning, Anshan  
114051, China

\*Corresponding authors E-mail: liuzunfeng@nankai.edu.cn (Z.L.), zhouxiang@cpu.edu.cn  
(X.Z.), lijingjing9009@126.com (J.L.)

#### **This file contains:**

Supplementary Notes S1 to S3

Supplementary Figures S1 to S39

Supplementary Tables S1 to S5

Supplementary Captions for Movies S1 to S4

References for SI reference citations

Other supplementary materials for this manuscript include the following:

Supplementary Movies S1 to S4

## Supplementary Notes

### Note S1: Energy conversion efficiency of the PVDF-CB/PEA/PAM actuators

The conversion efficiency can be defined by the following Equation S1:

$$\eta = \frac{E_{out}}{E_{in}} \quad (S1),$$

where  $E_{in}$  and  $E_{out}$  are given by the following equations:<sup>1</sup>

$$E_{in} = P \cdot A \cdot t \quad (S2),$$

$$E_{out} = \frac{[E_s H_s^2 (3H_f + H_s) + E_f H_f^2 (3H_s + H_f)] \times [E_f^2 H_f^4 + E_s^2 H_s^4 + 2E_s E_f H_f H_s (2H_f^2 + 3H_f H_s + 2H_s^2)] \kappa^2}{36E_s E_f H_f^2 H_s^2 (H_s + H_f)} \quad (S3),$$

where the subscripts f and s represent the PAM film and PVDF-CB substrate layers, respectively.  $E$  is the Young's modulus,  $H$  is thickness and  $\kappa$  is bending curvature.

At 250 mW/cm<sup>2</sup> NIR light illumination, the bending radius and responsive time are ~2.3 cm<sup>-1</sup> and 0.6 s, respectively, and the parameters for the above equation are listed below:  $E_f = 2452$  MPa;  $E_s = 800$  MPa;  $H_f = 3 \times 10^{-5}$  m;  $H_s = 6 \times 10^{-5}$  m. The elastic energy and the light energy are calculated to be 1.19 mJ and 22.5 mJ, respectively. Then the energy conversion efficiency is calculated to be 5.29%.

### Note S2: Transient heat-transfer analysis of the PVDF-CB/PEA/PAM actuators

The surface temperature of the PVDF-CB/PEA/PAM actuator increases on illumination with NIR light, and a transient heat transfer analysis is conducted to quantify the temperature change as a function of light intensity and irradiation time. The heat conduction inside the actuator is very fast due to their small thicknesses. Therefore, the temperature distribution in the actuator is essentially uniform, and the analytical expression for the temperature can be deduced by considering the irradiating light as a surface heat flux, the heat-convection relationship with the surrounding air, and the energy equilibrium. The corresponding expression for temperature as a function of time is given by the equation S4:

$$\Delta T(t) = T(t) - T_0 = \frac{2Pt}{\sum_i c_i \rho_i d_i + 2h_c t} \quad (S4),$$

where  $P$  is the light intensity;  $c_i$ ,  $\rho$ , and  $d_i$  are the specific heat capacity, volumetric mass density, and thickness, respectively, of the  $i^{\text{th}}$  layer; and  $h_c$  is the convective heat transfer coefficient of the air. The value of  $h_c$  depends on many factors such as relative velocity, and it can be varied from 10 to 100 W (m<sup>2</sup> K)<sup>-1</sup> or more.<sup>2</sup>

To verify the expression, we simulated the surface temperature of the PVDF-CB/PEA/PAM actuating film as a function of time at a specific light intensity when they are

free. The convective heat transfer coefficient here we used is  $10 \text{ W (m}^2 \text{ K)}^{-1}$ . The specific heat capacity of each layer of the PVDF-CB/PEA/PAM is measured to be 0.09, 1.3, and  $0.7 \text{ J g}^{-1} \text{ K}^{-1}$ , respectively, and the corresponding mass density is measured to be 1.5, 0.89, and  $0.48 \text{ g cm}^{-3}$ , respectively. By substituting all the parameters into the expression, the obtained theoretical values agree well with the experimental measurement (Figure S23), and the expression can be used to calculate the temperature change of the actuators at different light intensities.

### Note S3: Thermomechanical analysis of the PVDF-CB/PEA/PAM actuators

The mechanical properties of each layer of the PVDF-CB/PEA/PAM film were first measured for understanding their mechanical function on the bending actuation. The moduli of the individual layers were calculated by using the rule of mixture for composites, i.e., equation S5,

$$E^H = \sum_{i=1}^N f_i E_i \quad (\text{S5}),$$

in which  $E^H$  is the effective modulus of the composite film, and  $f_i$  and  $E_i$  are the volume fraction and Young's modulus, respectively, of the  $i^{\text{th}}$  constituent. The calculated Young's moduli of the PVDF-CB layer, the PEA layer, and the PAM hydrogel layer were calculated to be about 800 MPa, 150 MPa, and 2452 MPa, respectively.

The excellent actuation performance of the PVDF-CB/PEA/PAM actuator is induced by the mismatch in expansion between the different layers upon heating due to light irradiation, including the thermal expansion of the PVDF-CB film, and the thermal contraction of the PAM hydrogel layer due to the water loss. To quantitatively study the mechanism, a thermomechanical analysis was conducted by using the classical Timoshenko beam theory.<sup>3</sup> Under the assumptions of perfect bonding between layers and a uniform temperature distribution, the strain and stress distribution in the  $i^{\text{th}}$  layer that are derived using beam theory are given by Equation S6 and S7:

$$\varepsilon_i = \frac{\left(\frac{\gamma}{K_e} - c_i - z_i\right) \left(\frac{\gamma}{K_e} \sum_i F_i^* - \sum_i c_i F_i^*\right) + \sum_i F_i^*}{K_l + \beta - \frac{\gamma^2}{K_e}} \quad (\text{S6}),$$

$$\sigma_i = E_i (\varepsilon_i - \alpha_i \Delta T) \quad (\text{S7}),$$

in which  $z_i$  is the local coordinate in the thickness direction,  $\Delta T$  is the temperature change, and  $E_i$  and  $\alpha_i$  are the Young's modulus and the coefficient of thermal expansion, respectively, of

the  $i^{\text{th}}$  layer. The other constants are defined by the following Equation S8 and S9:

$$\gamma = \sum_i c_i E_i d_i, \beta = \sum_i c_i^2 E_i d_i, K_l = \sum_i E_i I_i K_e = \sum_i E_i d_i, I_i = \frac{d_i^3}{12}, F_i^* = E_i \alpha_i \Delta T d_i \quad (\text{S8}),$$

$$c_1 = 0, c_2 = \frac{d_1 + d_2}{2}, c_i = \frac{d_1 + d_i}{2} + \sum_{j=2}^{i-1} d_j \quad (i > 2) \quad (\text{S9}),$$

where  $d_i$  is the thickness of the  $i^{\text{th}}$  layer.

By employing the above transient heat-transfer analysis and thermomechanical analysis, we simulated the actuation temperature change and bending angle at different NIR light intensities, and the theoretical calculations show good agreement with the experimental data (Figure 2c).

## Supplementary figures

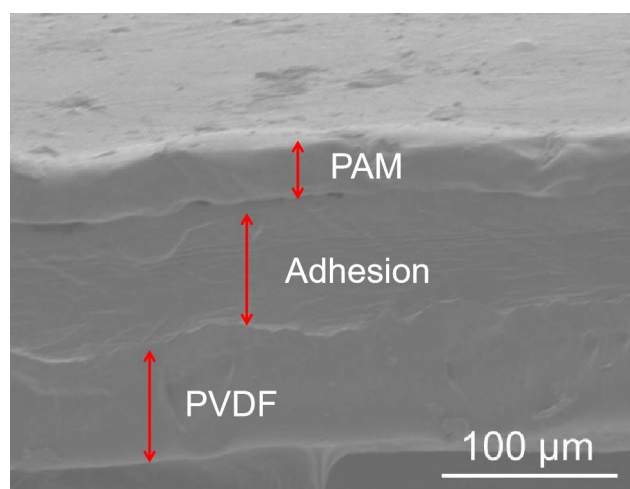


**Figure S1.** Cross-sectional SEM image of the PVDF-CB/PEA/PAM actuator.

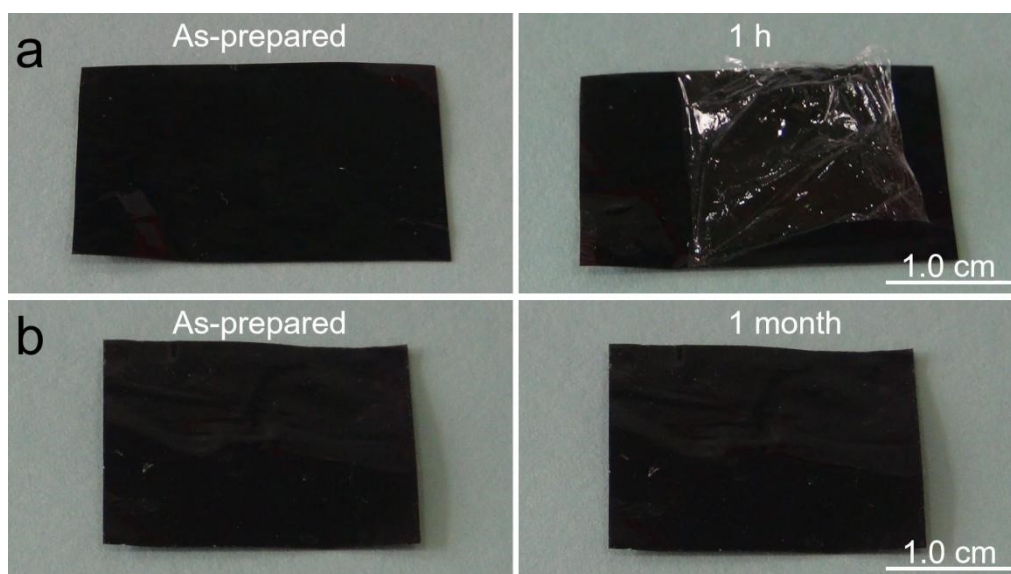


**Figure S2.** (a) Photographs of the PVDF-CB/PAM bilayer just prepared (left) and let stand for 1 h in air (right). (b) Photographs of the PVDF-CB/PEA/PAM tri-layer just prepared (left) and let stand for 1 month in air (right). This indicates the PVDF-CB/PEA/PAM trilayer film exhibits much higher interfacial stability than the PVDF-CB/PAM bilayer.

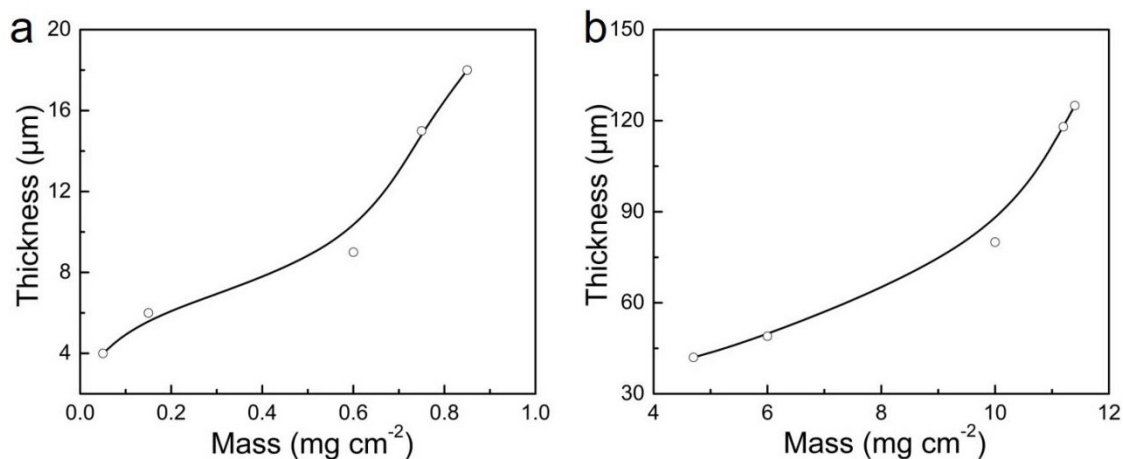


**Figure S3.** The thickness of the PAM (a) and the PEA (b) layers obtained by applying different amount of PAM gel and PEA solution by a “making-up” method.

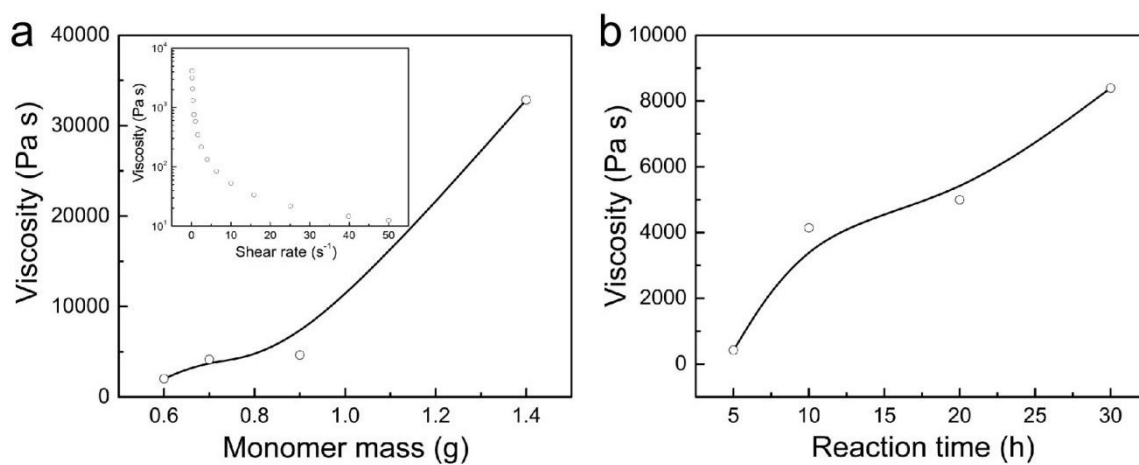


**Figure S4.** Viscosity of the PAM gel as a function of reaction time (a) and monomer mass (b). The inset in (a) shows viscosity as a function of shear rate. The reaction time is 10 h for (a), and the monomer concentration is 0.07 g/mL for (b).

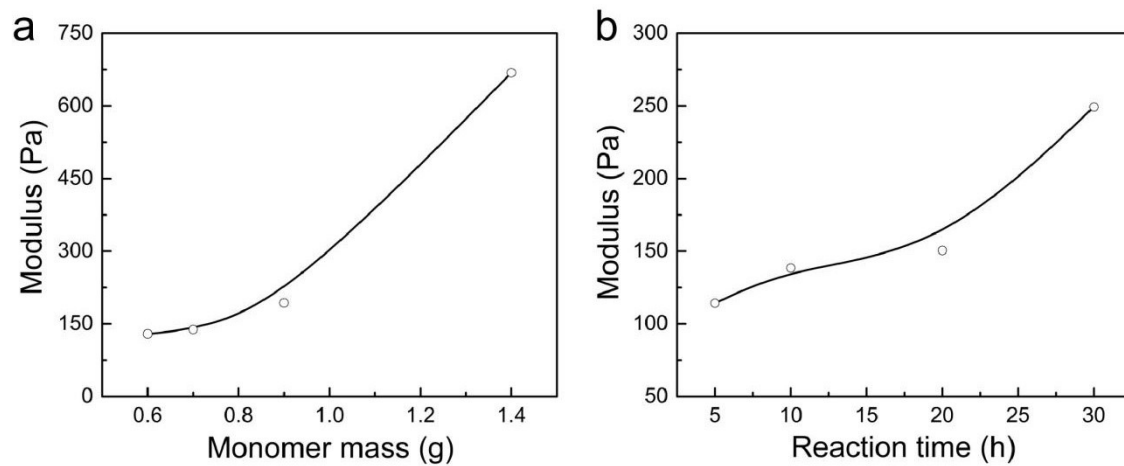


**Figure S5.** Modulus of the PAM gel as a function of reaction time (a) and monomer mass (b). The reaction time is 10 h for (a), and the monomer concentration is 0.07 g/mL for (b).

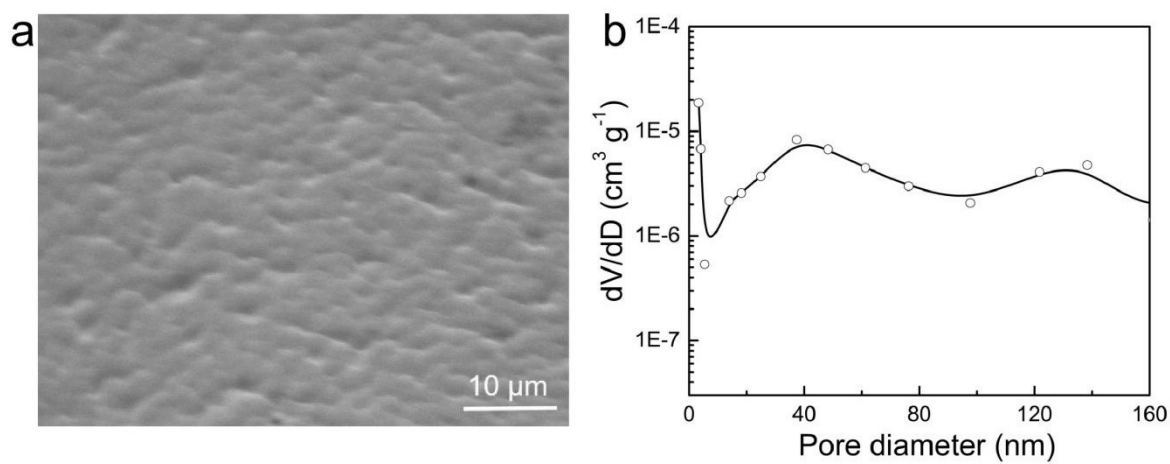


**Figure S6.** (a) SEM image and (b) the pore size distribution of the PVDF-CB film.

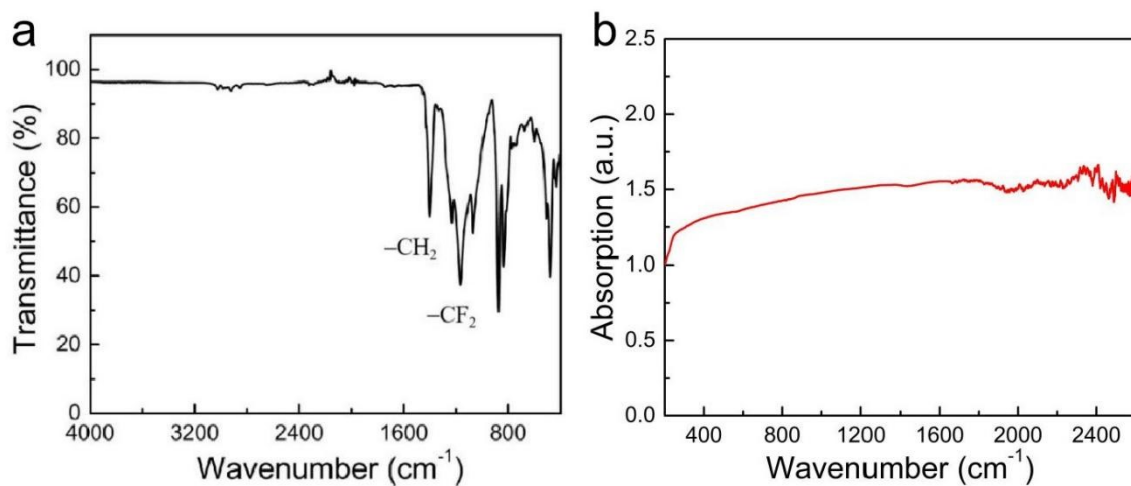


**Figure S7.** (a) FTIR and (b) UV-Vis-NIR spectrum of the PVDF-CB film.

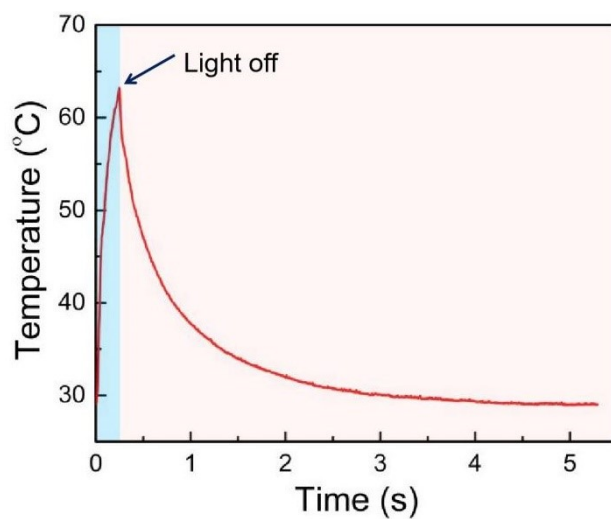


**Figure S8.** Temperature as a function of time of the PVDF-CB film by switching on and off 200 mW cm<sup>-2</sup> NIR light.

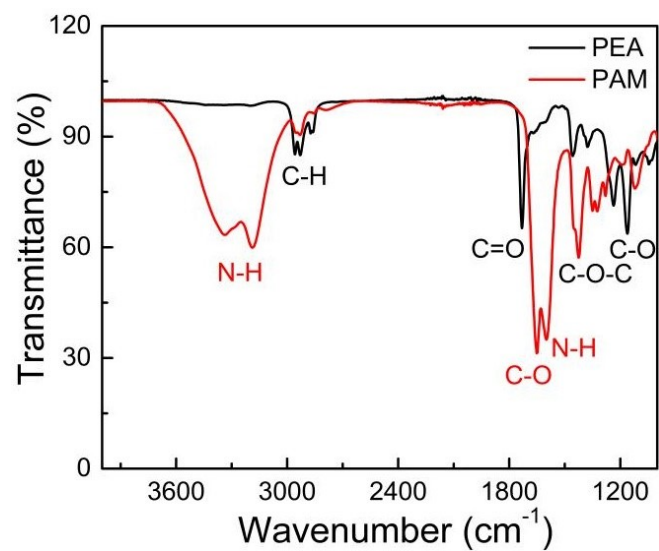


**Figure S9.** FTIR spectra of the PEA and the PAM layer (free-dried).

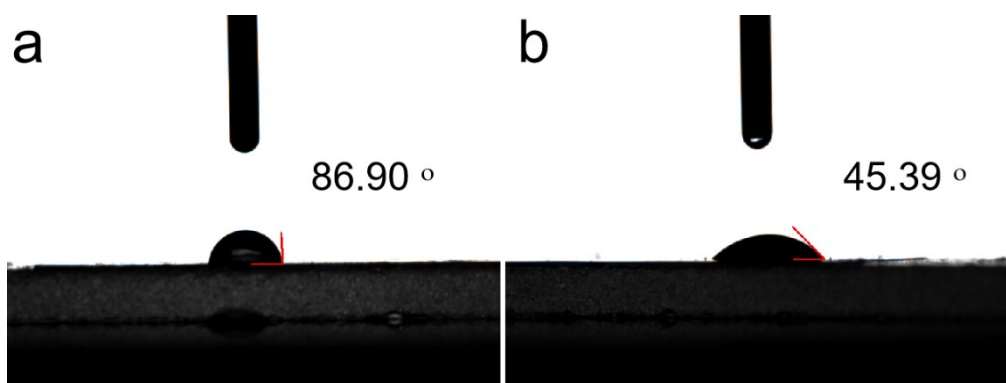


**Figure S10.** Photographs showing the water contact angle of the PVDF-CB layer (a) and the PAM layer (b).

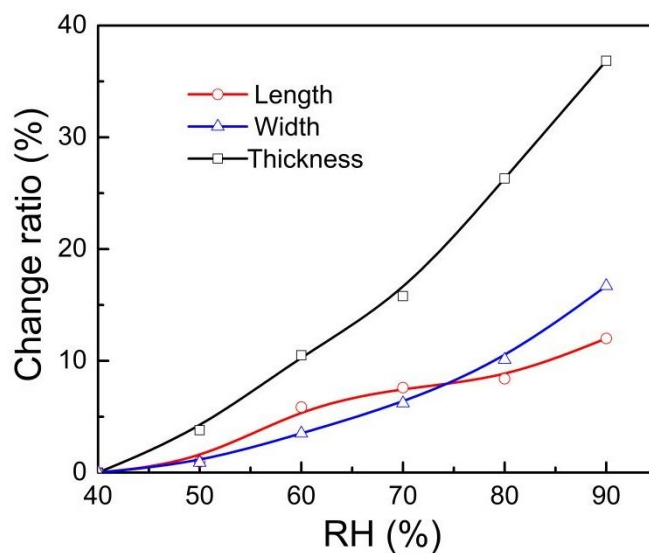


**Figure S11.** The change in length, width, and thickness as a function of environmental relative humidity (RH) for the PAM film (3 mm × 2 mm × 10 μm).

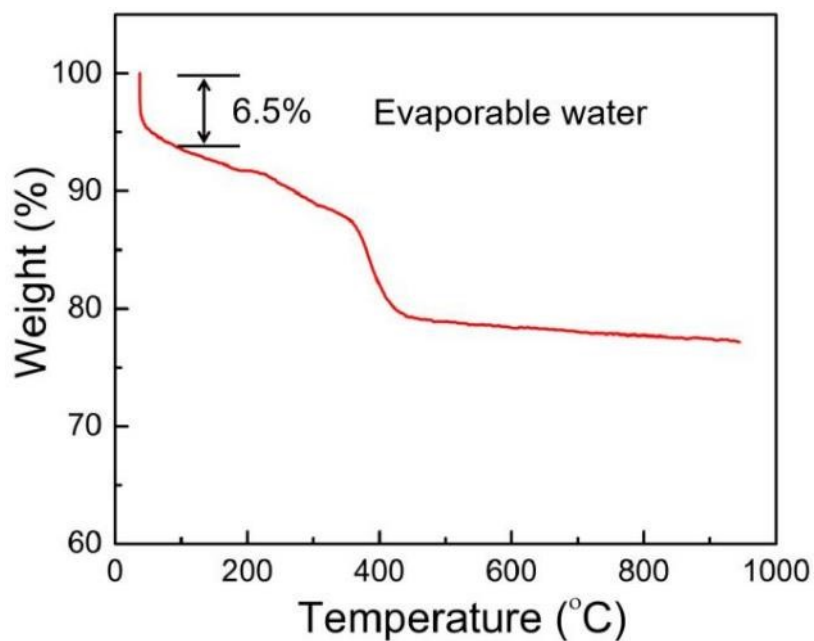


**Figure S12.** Thermogravimetric analysis (TGA) of a PAM film.

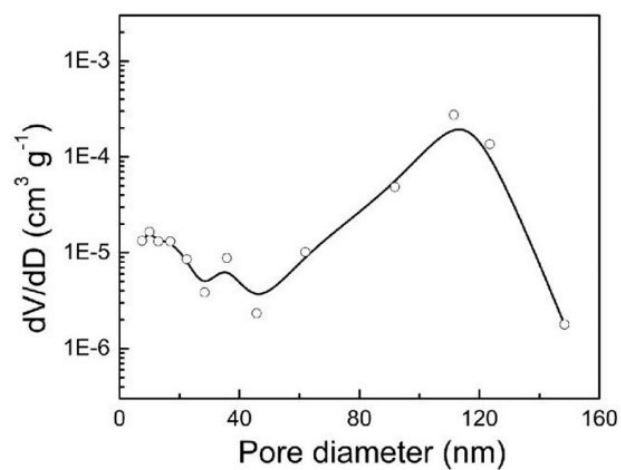


**Figure S13.** Pore size distribution of the freeze-dried PAM film.



**Figure S14.** Photographs of the PAM film (a) before and (b) after absorption of water moisture.

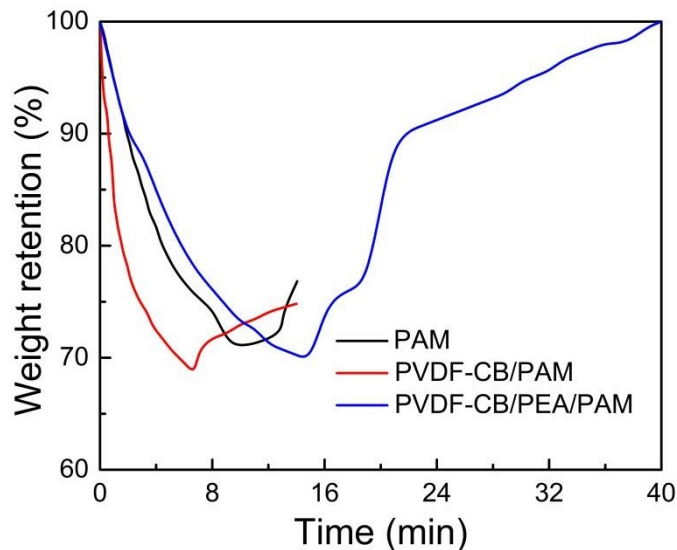


**Figure S15.** The weight retention with time of the PAM, PVDF-CB/PAM, and the PVDF-CB/PEA/PAM films by switching on and off  $250 \text{ mW cm}^{-2}$  NIR light. The environmental relative humidity is about 40%. The thicknesses of the PVDF-CB, PEA, and PAM layers are  $40 \mu\text{m}$ ,  $30 \mu\text{m}$ , and  $20 \mu\text{m}$ . Delamination was observed during the measurement for the PVDF-CB/PAM bilayer.

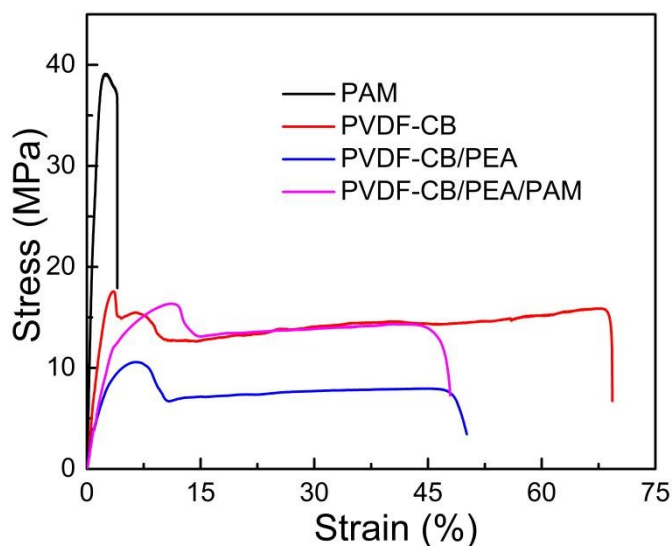


**Figure S16.** Stress-strain curves of the PVDF-CB film, PAM, PVDF-CB/PEA bilayer (thickness of each layer:  $60 \mu\text{m}/60 \mu\text{m}$ ), and the PVDF-CB/PEA/PAM tri-layer (thickness of every layer:  $60 \mu\text{m}/60 \mu\text{m}/30 \mu\text{m}$ ). If not specified, the PAM layer was obtained by peeling off from the PVDF-CB/PEA bilayer, and the same thickness of different layers were used in this and the following figures.

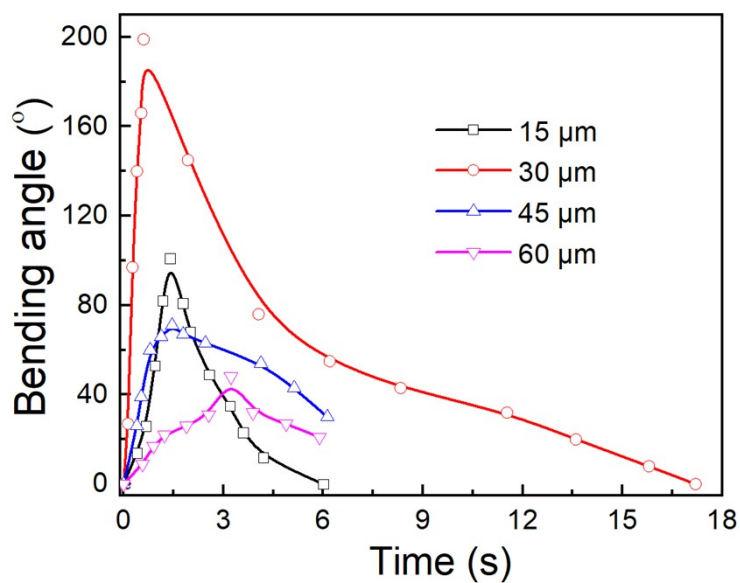


**Figure S17.** Bending angle as a function of time of the actuator with different thickness of the PAM layer. The thickness of the PVDF-CB layer is 60  $\mu\text{m}$ .



**Figure S18.** Photographs of the PVDF-CB/PEA/PAM actuator (a) before NIR light irradiation, (b) reaching the maximum angle by switching on the light irradiation, and (c) after switching off light irradiation.

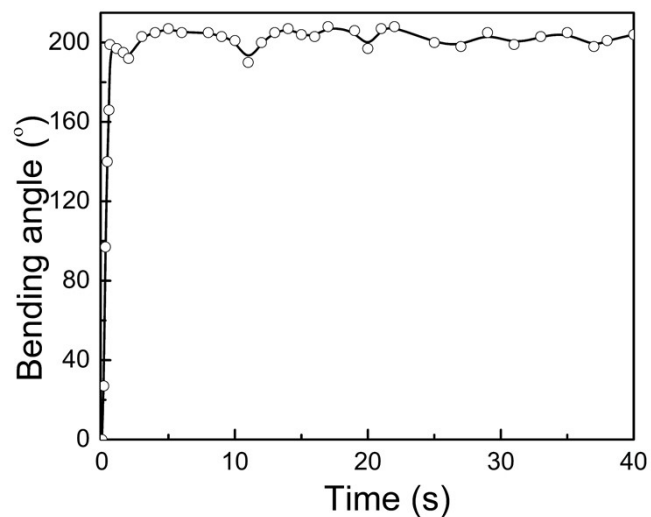


**Figure S19.** Bending angle as a function of time for the 150  $\mu\text{m}$  PVDF-CB/PEA/PAM actuator under 250  $\text{mW cm}^{-2}$  NIR light irradiation.

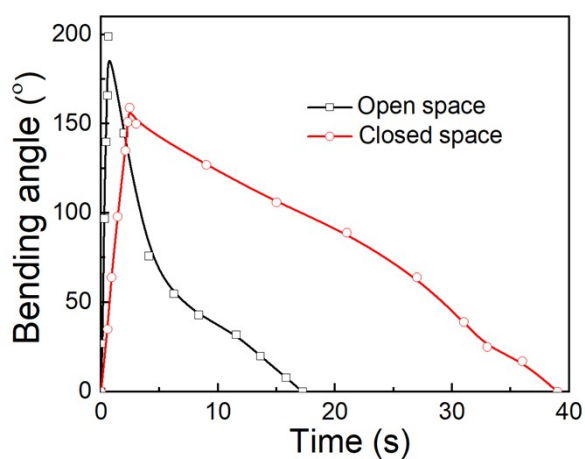


**Figure S20.** Bending angle as a function of time of the PVDF-CB/PEA/PAM actuator in an open and closed space.

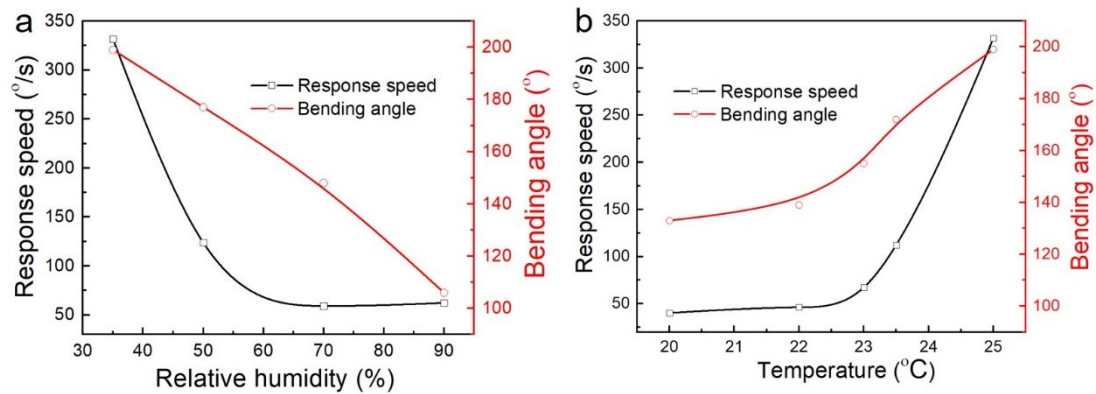


**Figure S21.** Response time and bending angle of the PVDF-CB/PEA/PAM actuator as a function of (a) relative humidity and (b) environmental temperature.

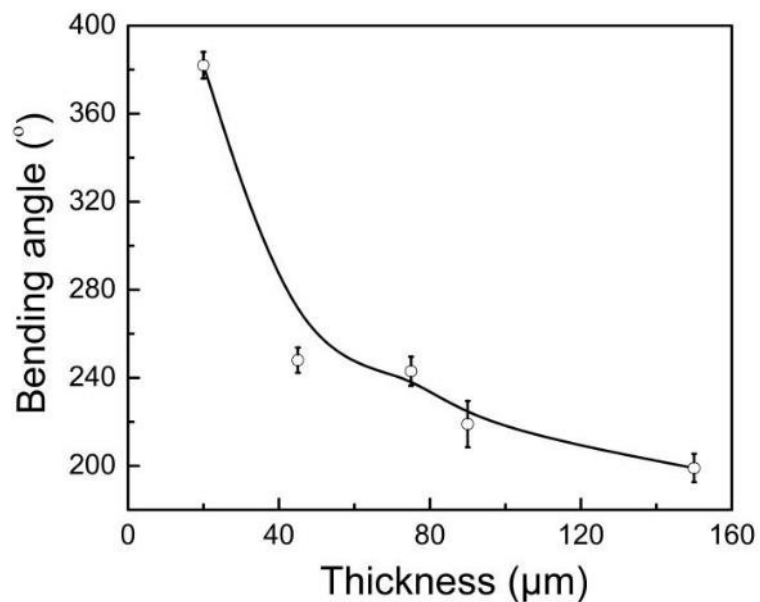


**Figure S22.** Bending angle as a function of thickness of the PVDF-CB/PEA/PAM actuator under illumination of 250 mW cm<sup>-2</sup> NIR light.

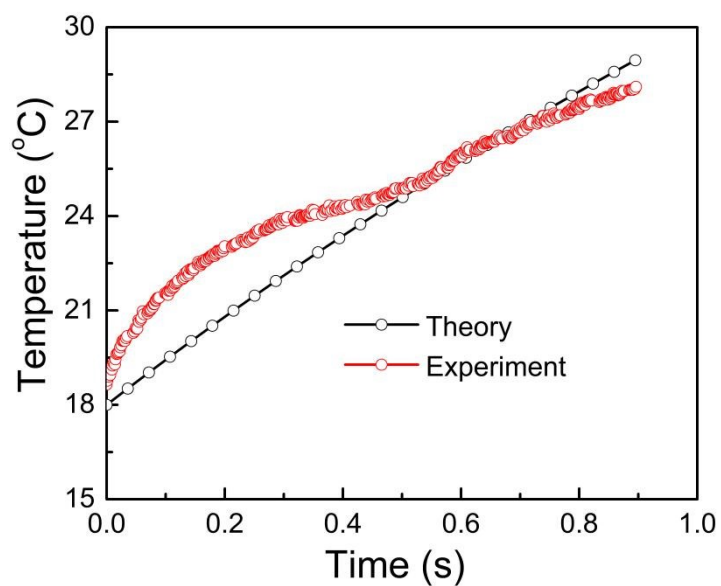


**Figure S23.** Experimentally measured and theoretically calculated temperatures of the PVDF-CB/PEA/PAM actuator as a functions of time. The light intensity was  $68 \text{ mW cm}^{-2}$ .

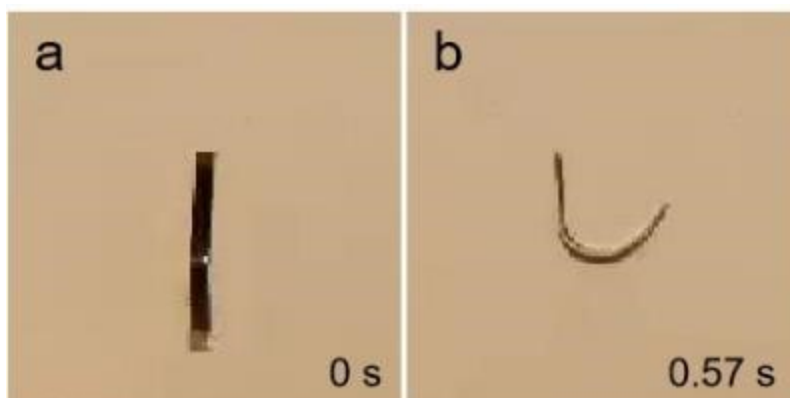


**Figure S24.** Photographs of a 20- $\mu\text{m}$ -thick PVDF-CB/PEA/PAM actuator before (a) and after (b) exposure to the sunlight.

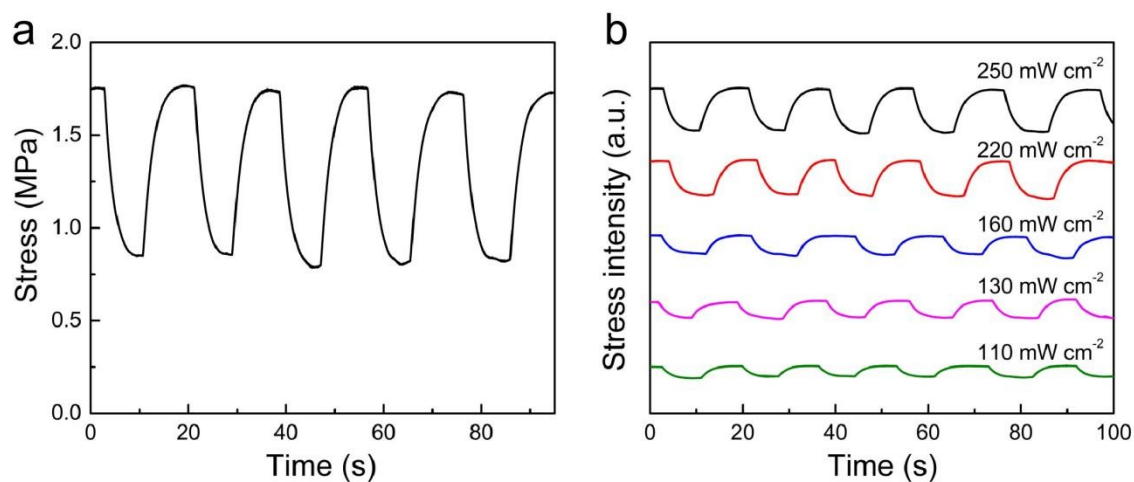


**Figure S25.** (a) Stress as a function of time for the 150  $\mu\text{m}$  PVDF-CB/PEA/PAM film under 250  $\text{mW cm}^{-2}$  NIR light. (b) Actuation stress of the 150  $\mu\text{m}$  PVDF-CB/PEA/PAM film at different light intensities.

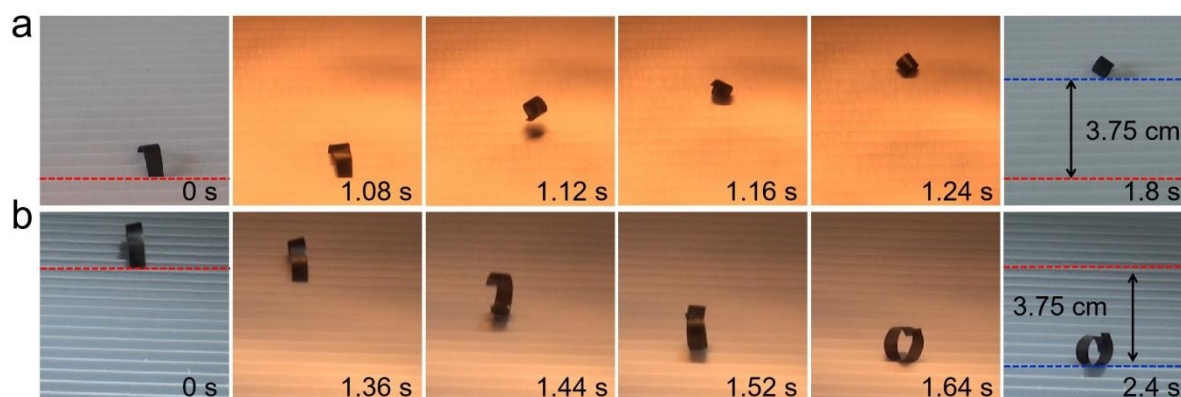


**Figure S26.** Schematic and photographs showing the PVDF-CB/PEA/PAM actuator jumping up and forward (a) or backward (b) in response to 200  $\text{mW cm}^{-2}$  NIR light on a zig-zag surface.

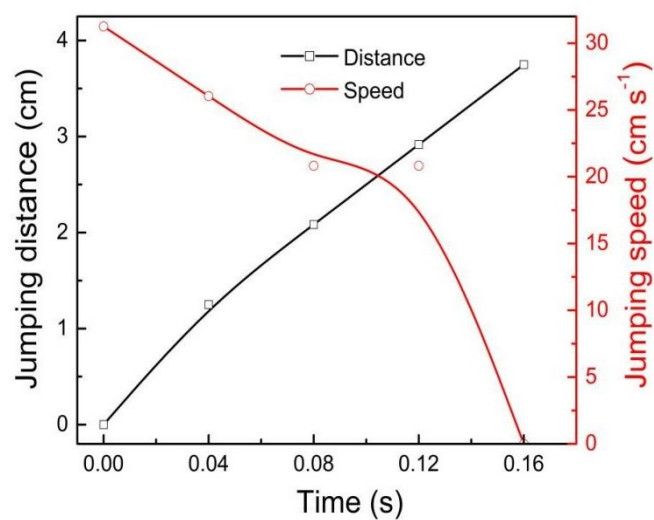


**Figure S27.** The jumping translational distance, and speed of the PVDF-CB/PEA/PAM jumping actuator as a function of time obtained from Figure 18a.

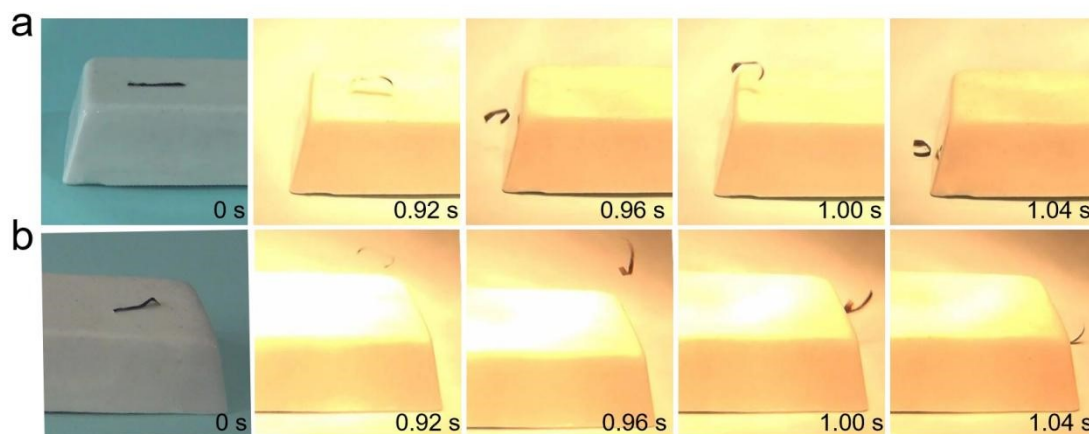


**Figure S28.** Schematic and photographs showing an asymmetric PVDF-CB/PEA/PAM actuator jumping up and forward (a) or backward (b) in response to 250 mW cm<sup>-2</sup> NIR light on a flat surface.

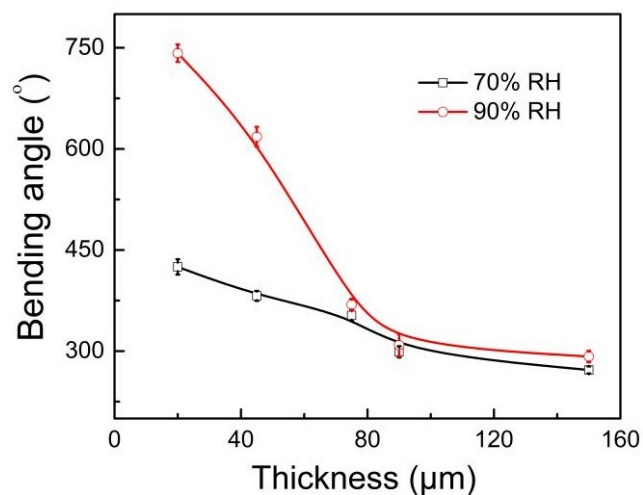


**Figure S29.** Bending angle as a function of thickness of the PVDF-CB/PEA/PAM at 70% and relative humidity.

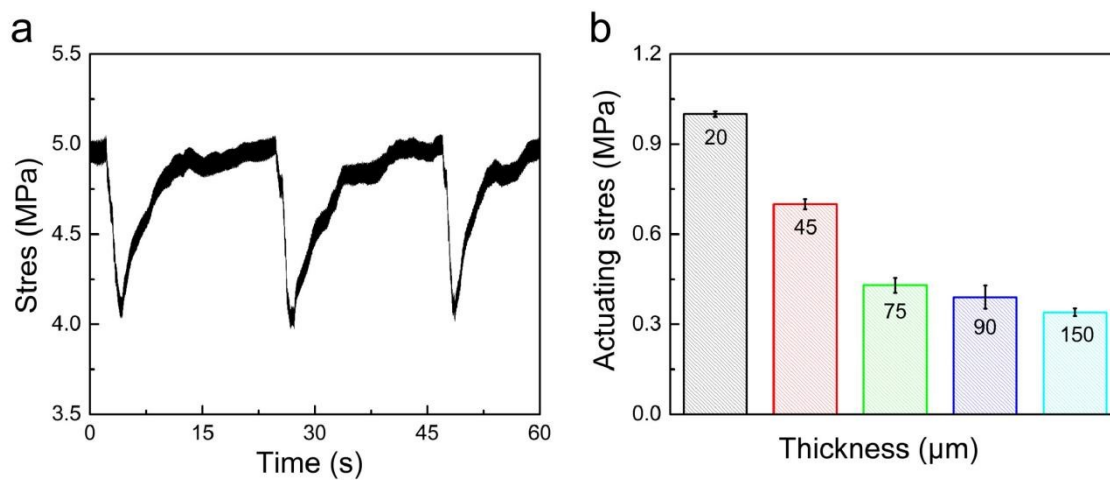


**Figure S30.** (a) Stress as a function of time by applying and removing moisture (with flux of  $15 \text{ mg s}^{-1}$ ) for a 20- $\mu\text{m}$ -thick PVDF-CB/PEA/PAM film that is stained on a mechanical tester. (b) Actuation stress as a function of thickness of the PVDF-CB/PEA/PAM film.

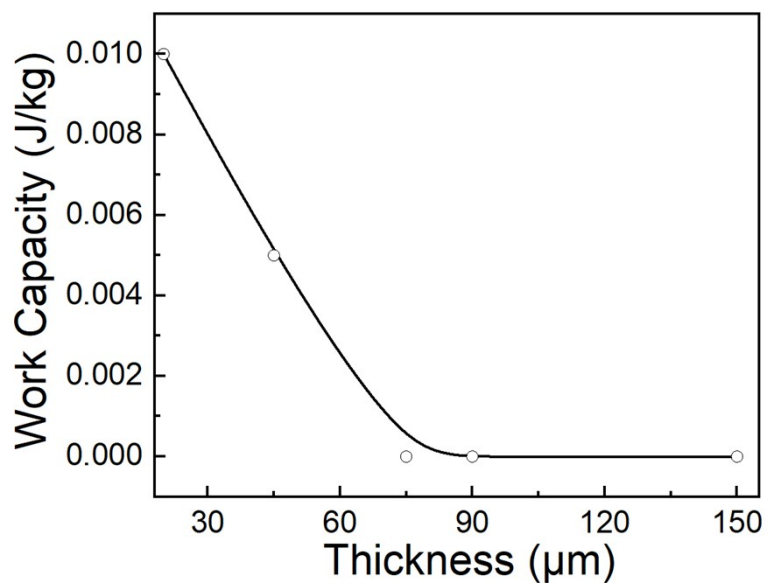


**Figure S31.** Work capacity as a function of thickness for the actuator under moisture stimuli.

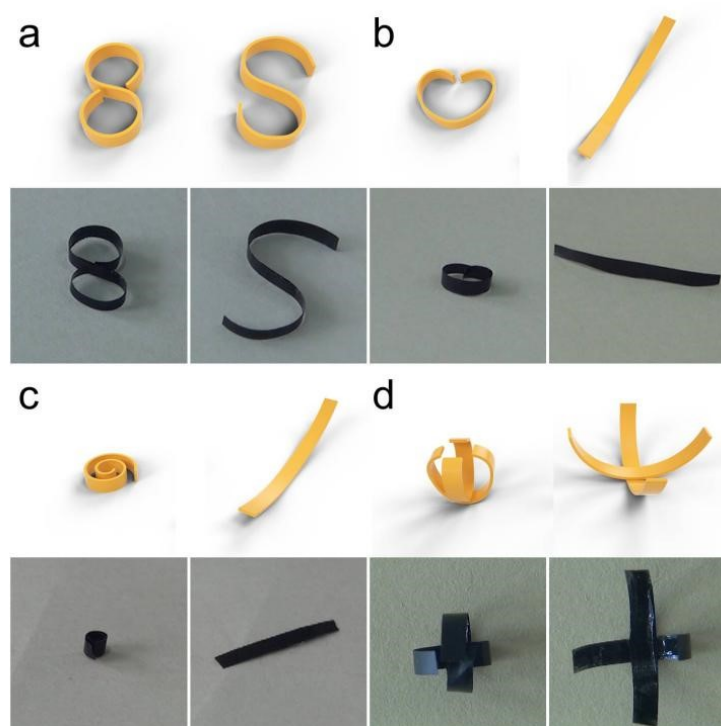


**Figure S32.** Schematic and photographs showing multi-morphing actuation of the PVDF-CB/PEA/PAM actuators in response to moisture. (a) A number-“8”-shape extended to a letter “S” shape. (b) A heart-shape extended to straight film. (c) A spiral shape extended to straight film. (d) The actuator mimicking the flower blooming.

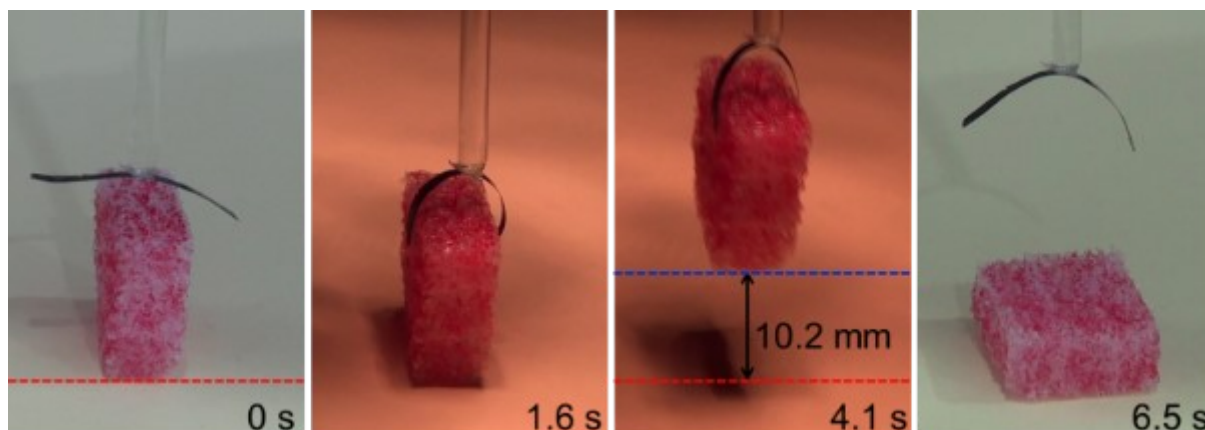


**Figure S33.** Photographs showing a PVDF-CB/PEA/PAM actuator grasping and lifting a foam that is 78 times its own weight in response to  $250 \text{ mW cm}^{-2}$  NIR light.

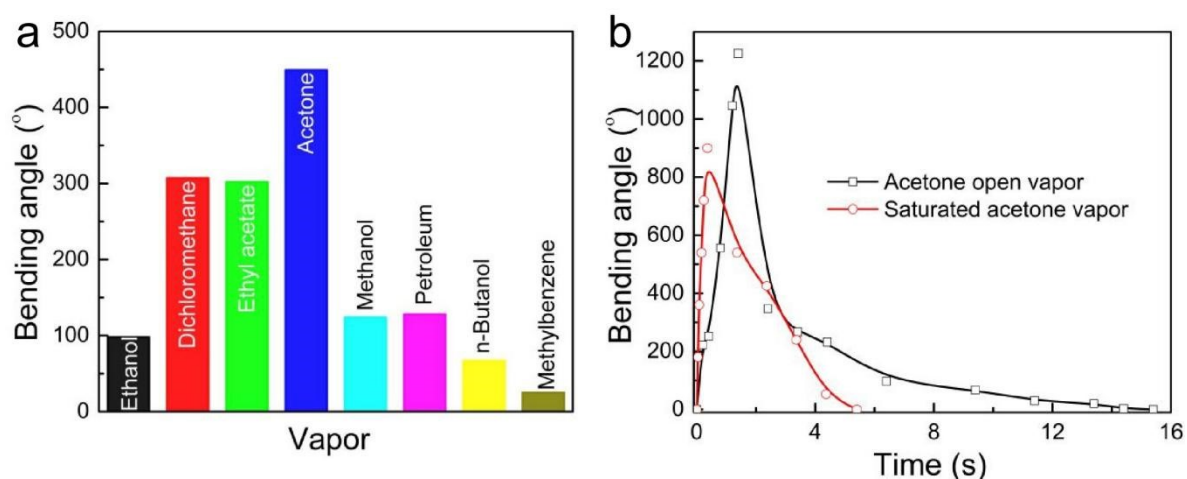


**Figure S34.** (a) Maximum bending angle for the  $150 \mu\text{m}$  PVDF-CB/PEA/PAM actuator at 15 mm above an open beaker that contains different organic vapors. (b) Bending angle as a function of time for a  $20\text{-}\mu\text{m}$ -thick PVDF-CB/PEA/PAM actuator by applying or removing the acetone vapor (saturated vapor or 15 mm above an open beaker that contains acetone).

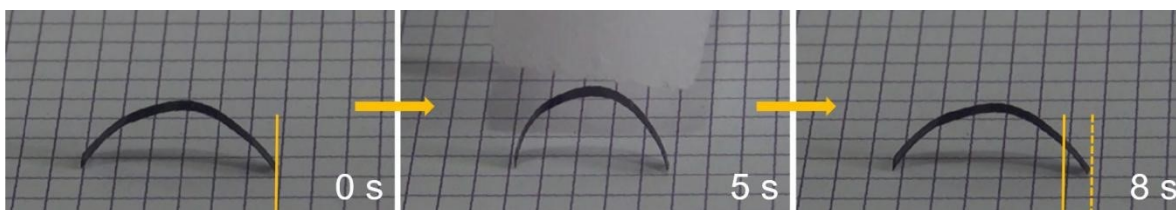


**Figure S35.** Photographs showing a PVDF-CB/PEA/PAM actuator walked forward in response to ethanol vapor.

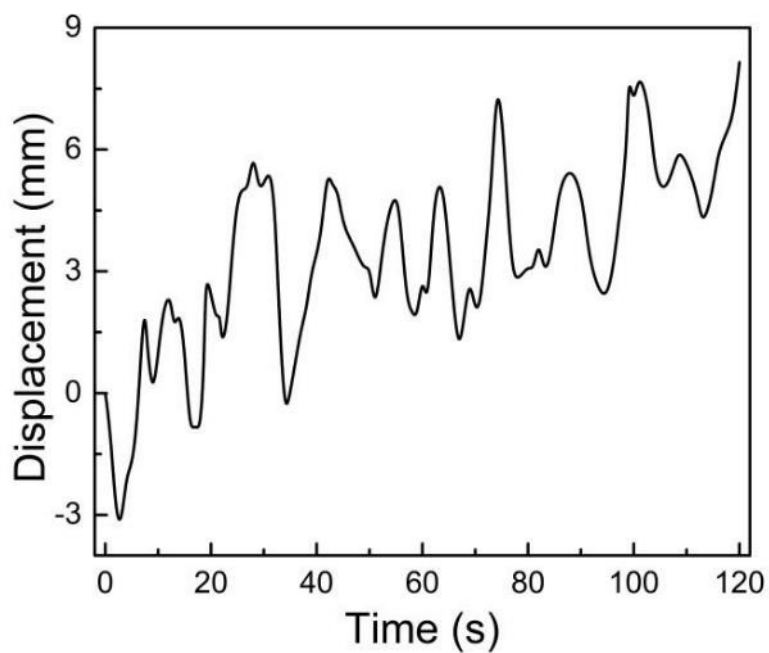


**Figure S36.** Oscillation actuation as a function of time of a 20- $\mu\text{m}$ -thick PVDF-CB/PEA/PAM actuator in environmental conditions.



**Figure S37.** Photographs showing oscillatory swing of a curved PVDF-CB/PEA/PAM actuator placed on the surface.

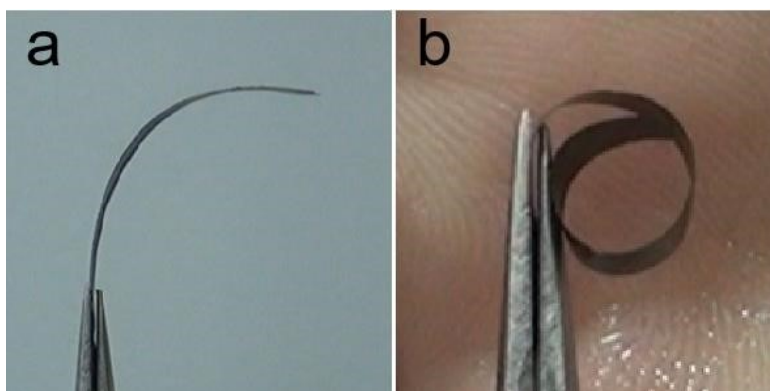


**Figure S38.** Photographs showing the PVDF-CB/PEA/PAM actuator (a) bends into a highly curved circle by approaching the palm (b) because of the increased humidity close to the palm. The PAM layer is in the outside of the curve.

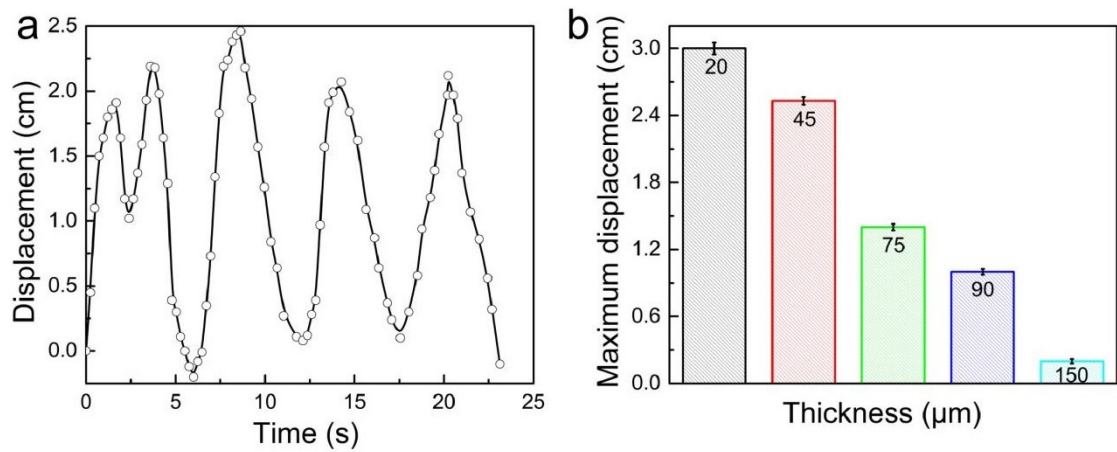


**Figure S39.** (a) The oscillation displacement as a function of time for a 20- $\mu\text{m}$ -thick PVDF-CB/PEA/PAM actuator at 5 mm above a palm. (b) The maximum oscillation displacement of the PVDF-CB/PEA/PAM actuator with different thicknesses at 5 mm above a palm.

## Supplementary Tables:

**Table S1.** Comparison of the actuation performances of the PVDF-CB/PEA/PAM actuator in response to NIR light with typical literature reported light-driven actuators that the actuation performance parameters can be obtained.

Material	Thickness $d$ ( $\mu\text{m}$ )	Curvature $\kappa$ ( $\text{cm}^{-1}$ )	Response time $t$ (s)	$\Delta T$ ( $^{\circ}\text{C}$ )	$t/d$ ( $\text{s } \mu\text{m}^{-1}$ )	$\kappa \times d / \Delta T$ $10^{-4} (^{\circ}\text{C})^{-1}$	$\kappa \times d / (t \times \Delta T)$ $10^{-4} (\text{s } ^{\circ}\text{C})^{-1}$	Ref.
PVDF-CB/PEA/PAM	150	2.3	0.6	34.7	0.004	9.94	16.57	This work
PVDF-CB/PEA/PAM	20	4.44	0.56	10.5	0.028	8.46	15.10	This work
MXene/PE	42	4.0	2.1	29	0.05	5.79	2.76	4
IPAT-2	5	7.6	0.36	9.9	0.072	3.84	10.67	5
IrGO/GO	5.5	6.9	13.2	45	2.4	0.85	0.06	6
MXene/Cellulose	20	0.84	6.6	54.5	3.3	0.31	0.05	7
BOPP/graphite/paper	67	1.9	10	41.4	0.15	3.07	0.31	8
GO-PDA/rGO	2.4	2.09	2	31.8	0.83	0.16	0.08	9
PE/CNT	40	5.0	1.4	28.8	0.035	6.94	4.96	10
PDMS/CNT	111	1.5	0.83	42.4	0.007	3.93	4.73	11
PC/CNT	11	0.63	0.87	25	0.079	0.28	0.32	3
PI/paraffin wax/CNT	33	0.74	0.87	20	0.026	1.22	1.40	12

GO: graphene oxide; IrGO: Iodine-doped reduced graphene oxide; rGO: reduced graphene oxide; BOPP: biaxially oriented polypropylene; CNT: carbon nanotube; CNF: cellulose nanofibrils; PDA: polydopamine; PE: polyethylene; PC: polycarbonate; PI: polyimide. IPAT: ink-PET-acrylic.

**Table S2.** Comparison of the actuation performances of the PVDF-CB/PEA/PAM jumping actuator with literature reported jumping actuators.

Material	Initial speed ( $\text{cm s}^{-1}$ )	Height (mm)	Response time (s)	Direction control	Work ( $\text{J Kg}^{-1}$ )	Light stimuli	Vapor stimuli	Ref.
PVDF-CB/PEA/PAM	56	4.5	0.16	Yes	0.16	Yes	-	This work
PVDF-CB/PEA/PAM	51.4	13.2	0.08	No	0.13	-	Yes	This work
PDMS/CNT	79	32	0.92	No	0.31	Yes	No	11
CNP	44	10	0.36	No	0.098	Yes	No	13
GO-CNT	20	0.84	6.6	No	0.05	Yes	No	14
LCE-CNT	125	80	0.05	Yes	0.78	Yes	No	15
azo-LCN	88	31	0.062	Yes	0.39	Yes	No	16
PIQA/CNS	71	26	0.13	No	0.25	No	Yes	17

GO: graphene oxide; PIQA: poly(indenoquinacridone); CNS: carbon nanotube sheet; CNT: carbon nanotube; CNP: carbon nitride polymer; LCE/LCN: liquid crystal elastomer/network.

**Table S3.** Comparison of the actuation performances of the PVDF-CB/PEA/PAM actuator with typical literature reported humidity-responsive actuators.

Material	Thickness $d$ ( $\mu\text{m}$ )	Bending angle $\theta$ ( $^\circ$ )	Response time $t$ (s)	$t/d$ (s $\mu\text{m}^{-1}$ )	$\theta \times d$ ( $^\circ \mu\text{m}$ )	$\theta/t$ ( $^\circ \text{s}^{-1}$ )	$\theta \times d/t$ ( $^\circ \mu\text{m s}^{-1}$ )	Ref.
PVDF-CB/PEA/PAM	20	742	14	0.7	14840	53	1060	This work
PVDF-CB/PEA/PAM	20	165	0.04	0.002	3300	4125	82500	This work
PVDF-CB/PEA/PAM	20	215	0.48	0.024	4300	448	8958	This work
PVDF-CB/PEA/PAM	20	220	0.16	0.008	4400	1375	27500	This work
PVDF-CB/PEA/PAM	20	130	0.12	0.006	2600	1083	21667	This work
PVDF-CB/PEA/PAM	20	395	0.2	0.01	7900	1975	39500	This work
PVDF-CB/PEA/PAM	20	930	2.08	0.104	18600	447	8942	This work
PVDF-CB/PEA/PAM	150	292	16	0.106	43800	18.25	2738	This work
GO/rGO	40	170	25	0.625	6800	6.8	272	18
BOPP/graphite/paper	67	292	60	0.895	19564	4.87	326	8
CLCP	14	180	0.4	0.029	2520	450	6300	19
CS/GO	40	180	4.5	0.113	7200	40	1600	20
SGO/rGO	4.6	194	6.8	14.78	894	28.53	131	21
GO	12	160	15	1.25	1920	10.67	128	22
IrGO/GO	5.5	280	419	76.18	1540	0.67	3.7	6
GO-CNT	0.8	350	0.08	0.1	280	4375	3500	14
MXene/CNF/PDA	10	319	11.1	1.11	3190	28.74	287.4	23
PA100-LCN	80	289	10	0.125	23120	28.9	2312	24
CCOs/PVDF	15	348.6	0.3	0.02	5229	1162	17430	25
MXene/BC	11	176	1.6	0.145	1936	110	1210	26
AG/LGF@AG	60	135	2	0.033	8100	4090	4050	27
SA/PVDF	70	110	14	0.2	7700	7.86	550	28

GO: graphene oxide; rGO: reduced graphene oxide; BOPP: biaxially oriented polypropylene; CLCP: cross-linked LC polymer; CS: chitosan; SGO: small flakes of graphene oxide; IrGO: Iodine-doped reduced graphene oxide; CNT: carbon nanotube; CNF: cellulose nanofibrils; PDA: polydopamine; PA: poly(acrylic-co-hydroxyethyl acrylate); COOs:  $\text{CaCO}_3$  oligomers; PVDF: polyvinylidene fluoride; BC: bacterial cellulose; SA: sodium alginate; LGF: longitudinal glass fibers; AG: agarose.

**Table S4.** The actuation bending angle for the PVDF-CB/PEA/PAM actuators by approaching to 15 mm above an open beaker that contains different solvents. The polarity and the saturated vapor pressure are also listed in the table.

Solvent	Polarity	Saturated vapor pressure (kPa)	Bending angle (°)
Dichloromethane	3.1	53.3	307
Ethyl acetate	4.4	14	304
Acetone	5.1	30.5	449
<i>n</i> -Butanol	3.7	0.8	67
Petroleum	0.01	53.3	128
Methylbenzene	2.4	14	25
Methanol	6.6	16.8	124
Ethanol	4.3	8.5	98

**Table S5.** Comparison of the actuation performances of the PVDF-CB/PEA/PAM actuator in response to acetone with literature reported actuators in response to organic vapors.

Material	Thickness $d$ ( $\mu\text{m}$ )	Bending angle $\theta$ (°)	Response time $t$ (s)	$\theta \times d$ (° $\mu\text{m}$ )	$\theta \times d/t$ (° $\mu\text{m s}^{-1}$ )	Stimulus	Ref.
PVDF- CB/PEA/PAM	20	1226	1.4	24520	17514	Acetone (saturated)	This work
PVDF- CB/PEA/PAM	20	900	0.36	18000	50000	Acetone (open)	This work
PIQA/CNS	8	315	0.04	2520	63000	CH <sub>2</sub> Cl <sub>2</sub>	17
PIQA/CNS	8	2880	9.17	23040	2512.5	CH <sub>2</sub> Cl <sub>2</sub>	17
PFSA	75	180	0.25	13500	54000	Ethanol	29
PILTf2N/C- pillar[5]arene	30	1080	0.3	32400	108000	Acetone	30
CCBM	26	300	5	7800	1560	Methanol	31
PIL- PAA@tissue paper	100	720	6	72000	12000	Acetone	32
GO/latex	150	1456	18	218400	12133	n-hexane	33
PVDF/PVA	40	860	3	34400	11466	Acetone	34

GO: graphene oxide; PIQA: poly(indenoquinacridone); CNS: carbon nanotube sheet; BOPP: biaxially oriented polypropylene; CLCP: cross-linked LC polymer; CS: chitosan; PFSA: perfluorosulfonic acid ionomer; CCBM: clay-clay bilayer membrane; PIL: poly(ionic liquid); PAA: poly(acrylic acid); PVDF: polyvinylidene fluoride; PVA: polyvinyl alcohol.

## Supplementary Movies:

**Movie S1.** A jumping robot based on the PVDF-CB/PEA/PAM actuator that can jump forward and backward on a zigzag substrate upon NIR irradiation ( $200 \text{ mW cm}^{-2}$ ). The actuator of  $20 \text{ mm} \times 1.5 \text{ mm} \times 20 \text{ }\mu\text{m}$  was used here. The actuator reached a maximum jumping translational distance of 37.5 mm in 160 ms. The initial velocity reached 0.56 m/s, generating a specific work capacity of 0.16 J/kg.

**Movie S2.** A jumping robot based on the  $20 \text{ }\mu\text{m}$  thickness PVDF-CB/PEA/PAM actuator that can jump forward and backward on a rough plane upon NIR irradiation ( $250 \text{ mW cm}^{-2}$ ). The actuator of  $10 \text{ mm} \times 1.5 \text{ mm} \times 20 \text{ }\mu\text{m}$  was used here.

**Movie S3.** A jumping robot based on the PVDF-CB/PEA/PAM actuator that can jump driven by water vapor. The actuator of  $20 \text{ mm} \times 1.5 \text{ mm} \times 20 \text{ }\mu\text{m}$  was used here. The actuator reached a maximum height of 13.2 mm in 80 ms. The average jumping speed is  $0.17 \text{ m s}^{-1}$ .

**Movie S4.** The PVDF-CB/PEA/PAM actuator that can realize grasping, walking, and self-oscillation. The mechanical grippers composed of PVDF-CB/PEA/PAM actuators ( $20 \text{ mm} \times 1 \text{ mm} \times 20 \text{ }\mu\text{m}$ ) being used to capture and release foam driven by NIR irradiation ( $200 \text{ mW cm}^{-2}$ ), and the weight-lifting ratio is about 78; The walking robot ( $15 \text{ mm} \times 1 \text{ mm} \times 75 \text{ }\mu\text{m}$ ) can locomote forward in response to the ethanol vapor; The PVDF-CB/PEA/PAM film ( $20 \text{ mm} \times 2 \text{ mm} \times 20 \text{ }\mu\text{m}$ ) that can generate self-oscillating actuation when it is placed at about 5 mm from the palm.

## References

- 1 X. B. Zhang, Z. B. Yu, C. Wang, D. Zarrouk, J. W. T. Seo, J. C. Cheng, A. D. Buchan, K. Takei, Y. Zhao, J. W. Ager, J. J. Zhang, M. Hettick, M. C. Hersam, A. P. Pisano and R. S. Fearing, *Nat. Commun.*, 2014, **5**, 2983.
- 2 J. Whitelaw, Convective Heat Transfer, URL, accessed: September, 2018.
- 3 S. P. Timoshenko, *J. Opt. Soc. Am.* 1925, **11**, 233.
- 4 Y. Hu, L. L. Yang, Q. Y. Yan, Q. X. Ji, L. F. Chang, C. C. Zhang, J. Yan, R. R. Wang, L. Zhang, G. Wu, J. Sun, B. Zi, W. Chen and Y. C. Wu, *ACS Nano*, 2021, **15**, 5294–5306.
- 5 J. J. Li, R. Zhang, L. L. Mou, M. Jung de Andrade, X. Y. Hu, K. Q. Yu, J. K. Sun, T. J. Jia, Y. Y. Dou, H. Chen, S. L. Fang, D. Qian and Z. F. Liu, *Adv. Funct. Mater.*, 2019, **29**, 1808995.

- 6 J. Yang, J. X. Zhang, X. L. Li, J. W. Zhou, Y. P. Li, Z. P. Wang, J. L. Cheng, Q. Guan and B. Wang, *Nano Energy*, 2018, **53**, 916–925.
- 7 G. F. Cai, J. H. Ciou, Y. Z. Liu, Y. Jiang and P. S. Lee, *Sci. Adv.*, 2019, **5**, eaaw7956.
- 8 M. C. Weng, P. D. Zhou, L. Z. Chen, L. L. Zhang, W. Zhang, Z. G. Huang, C. H. Liu and S. S. Fan, *Adv. Funct. Mater.*, 2016, **26**, 7244–7253.
- 9 J. K. Mu, C. Y. Hou, H. Z. Wang, Y. Li, Q. H. Zhang and M. F. Zhu, *Sci. Adv.*, 2015, **1**, e1500533.
- 10 L. P. Li, J. X. Meng, C. Y. Hou, Q. H. Zhang, Y. G. Li, H. Yu and H. Z. Wang, *ACS Appl. Mater. Interface*, 2018, **10**, 15122–15128.
- 11 Y. Hu, J. Q. Liu, L. F. Chang, L. L. Yang, A. F. Xu, K. Qi, P. Lu, G. Wu, W. Chen and Y. C. Wu, *Adv. Funct. Mater.*, 2017, **27**, 1704388.
- 12 J. Deng, J. F. Li, P. N. Chen, X. Fang, X. M. Sun, Y. S. Jiang, W. Weng, B. J. Wang and H. S. Peng, *J. Am. Chem. Soc.*, 2016, **138**, 225.
- 13 H. Arazoe, D. Miyajima, K. Akaike, F. Araoka, E. Sato, T. Hikima, M. Kawamoto and T. Aida, *Nat. Mater.*, 2019, **15**, 1084–1089.
- 14 H. Li and J. F. Wang, *ACS Appl. Mater. Interfaces*, 2019, **11**, 10218–10225.
- 15 C. Ahn, X. D. Liang and S. Q. Cai, *Adv. Mater. Technol.*, 2019, **4**, 1900185.
- 16 J. Jeon, J. C. Choic, H. Lee, W. Cho, K. Lee, J. G. Kim, J. W. Lee, K. I. Joo, M. Cho, H. R. Kim and J. J. Wie, *Mater. Today*, 2021, **49**, 97–106.
- 17 K. Q. Yu, X. Z. Ji, T. Y. Yuan, Y. Cheng, J. J. Li, X. Y. Hu, Z. F. Liu, X. Zhou and L. Fang, *Adv. Mater.*, 2021, **33**, 2104558.
- 18 D. D. Han, Y. L. Zhang, H. B. Jiang, H. Xia, J. Feng, Q. D. Chen, H. L. Xu and H. B. Sun, *Adv. Mater.*, 2015, **27**, 332–338.
- 19 Y. Y. Liu, B. Xu, S. T. Sun, J. Wei, L. M. Wu and Y. L. Yu, *Adv. Mater.*, 2017, **29**, 1604792.
- 20 Y. Q. Zhang, H. Y. Jiang, F. B. Li, Y. H. Xia, Y. Lei, X. H. Jin, G. Z. Zhang and H. J. Li, *J. Mater. Chem. A*, 2017, **5**, 14604–14610.
- 21 G. C. Xu, J. Chen, M. Zhang and G. Q. Shi, *Sensor. Actuat. B: Chem.*, 2017, **242**, 418–422.
- 22 Y. H. Ge, R. Cao, S. J. Ye, Z. Chen, Z. F. Zhu, Y. F. Tu, D. T. Ge and X. M. Yang, *Chem. Commun.*, 2018, **54**, 3126–3129.
- 23 J. Cao, Z. H. Zhou, Q. C. Song, K. Y. Chen, G. H. Su, T. Zhou, Z. Zheng, C. H. Lu and X. X. Zhang, *ACS Nano*, 2020, **14**, 7055–7065.
- 24 R. C. Lan, Y. Z. Gao, C. Shen, R. Huang, J. Y. Bao, Z. P. Zhang, Q. Wang, L. Y. Zhang and H. Yang, *Adv. Funct. Mater.*, 2021, **31**, 2010578.

- 25 Y. He, K. R. Kong, Z. X. Guo, W. F. Fang, Z. Q. Ma, H. H. Pan, R. K. Tang and Z. M. Liu, *Adv. Funct. Mater.*, 2021, **21**, 2101291.
- 26 L. Y. Yang, J. Cui, L. Zhang, X. R. Xu, X. Chen and D. P. Sun, *Adv. Funct. Mater.*, 2021, **31**, 2101378.
- 27 L. D. Zhang, S. Chizhik, Y. Z. Wen and P. Naumov, *Adv. Funct. Mater.*, 2016, **26**, 1040–1053.
- 28 L. D. Zhang, X. X. Qiu, Y. H. Yuan and T. Zhang, *ACS Appl. Mater. Interfaces*, 2017, **9**, 41599–41606.
- 29 J. K. Mu, G. Wang, H. P. Yan, H. Y. Li, X. M. Wang, E. L. Gao, C. Y. Hou, A. T. C. Pham, L. J. Wu, Q. H. Zhang, Y. G. Li, Z. P. Xu, Y. Guo, E. Reichmanis, H. Z. Wang and M. F. Zhu, *Nat. Commun.*, 2018, **9**, 590.
- 30 Q. Zhao, J. W. C. Dunlop, X. L. Qiu, F. H. Huang, Z. B. Zhang, J. Heyda, J. Dzubiella, M. Antonietti and J. Y. Yuan, *Nat. Commun.*, 2014, **5**, 4293.
- 31 R. K. Gogoi and K. Raidongia, *Adv. Mater.*, 2017, **29**, 1701164.
- 32 H. J. Lin, J. Gong, H. Miao, R. Guterman, H. J. Song, Q. Zhao, J. W. C. Dunlop and J. Y. Yuan, *ACS Appl. Mater. Interfaces*, 2017, **9**, 15148.
- 33 Y. L. Tan, Z. Y. Chu, Z. H. Jiang, T. J. Hu, G. Y. Li and J. Song, *ACS Nano*, 2017, **11**, 6843–6852.
- 34 L. D. Zhang, P. Naumov, X. M. Du, Z. G. Hu and J. Wang, *Adv. Mater.*, 2017, **29**, 1702231.